Supplement of Atmos. Chem. Phys., 20, 8083–8102, 2020
https://doi.org/10.5194/acp-20-8083-2020-supplement

Atmospheric Chemistry and Physics
Open Access
EGU

Supplement of

Seasonal impact of biogenic very short-lived bromocarbons on lowermost stratospheric ozone between 60° N and 60° S during the 21st century

Javier Alejandro Barrera et al.

Correspondence to: Alfonso Saiz-Lopez (a.saiz@csic.es) and Rafael Pedro Fernandez (rpfernandez@mendoza-conicet.gob.ar)

Table S1. CAM-chem performance metrics in reproducing (HCl+ClO) MLS stratospheric observations in the mean global (3.5 hPa), tropics (50 hPa), SH-MLs (50 hPa) and NH-MLs (50 hPa).

	Global mean (3.5 hPa)	SH-MLs (50 hPa)	Tropics (50 hPa)	NH-MLs (50 hPa)
Bias (ppb)	– 0.61	– 0.32	– 1.26	– 0.41
NMB (%)	– 2.0	– 2.1	– 19.3	– 3.0
NME (%)	2.0	3.0	19.1	3.8

Note: The statistical analysis has been performed for the annual mean modelled Cl_y^{LL} abundances and observations from the Microwave Limb Sounder (MLS) (HCl + ClO) data for the period 2005 and 2015 (Waters et al., 2006; Livesey et al., 2018). Units for the model - observation bias are ppb, while the normalized mean bias (NMB) and normalized mean error (NME) are shown in percentage.

Table S2. CAM-chem performance metrics in reproducing SBUV total ozone column (TOC) observations in the tropics, SH-MLs and NH-MLs.

	SH-MLs		Tropics		NH-MLs	
	TOC^{LL}	TOC^{LL+VSL}	TOC^{LL}	TOC^{LL+VSL}	TOC^{LL}	TOC^{LL+VSL}
Bias (DU)	6.47	– 1.14	– 0.48	– 2.50	7.74	2.67
NMB (%)	2.1	– 0.4	– 0.2	– 1.0	2.3	0.8
NME (%)	2.5	1.5	0.9	1.1	2.4	1.5

Note: The statistical analysis has been performed for the annual mean modelled total ozone column and observations from the Solar Backscatter Ultraviolet (SBUV) merged total ozone column data set for the period 1980 and 2015 (Frith et al., 2014, 2017). Units for the model - observation bias are DU, while the normalized mean bias (NMB) and normalized mean error (NME) are shown in percentage.

Table S3. Odd oxygen (O_x) loss rates reactions grouped by family

Family	Reaction	ΔO_x	Odd oxygen loss[§]
O_{x-Loss}	$O + O_3 \rightarrow 2\times O_2$	−2	$O_{x-Loss} = 2\times R_{O+O3} + R_{O1D+H2O}$
	$O(1D) + H_2O \rightarrow 2\times OH$	−1	
HO_{x-Loss}	$HO_2 + O \rightarrow OH + O_2$	−2[†]	$HO_{x-Loss} = 2\times(R_{HO2+O} + R_{HO2+O3})$
	$HO_2 + O_3 \rightarrow OH + 2\times O_2$	−2[†]	
NO_{x-Loss}	$NO_2 + O \rightarrow NO + O_2$	−2	$NO_{x-Loss} = 2\times(R_{NO2+O} + J_{NO3})$
	$NO_3 + h\nu \rightarrow NO + O_2$	−2	
$Halog_{x-Loss}$	$ClO + O \rightarrow Cl + O_2$	−2	$ClO_{x-Loss} = 2\times(R_{ClO+O} + J_{CL2O2} + R_{ClO+ClO}{}^{a} + R_{ClO+ClO}{}^{b} + R_{ClO+HO2})$
	$Cl_2O_2 + h\nu \rightarrow 2\times Cl + O_2$	−2	
	$ClO + ClO \rightarrow Cl_2 + O_2$	−2	
	$ClO + ClO \rightarrow Cl + OclO$	−2	
	$ClO + HO_2 \rightarrow HOCl + O_2$	−2[£]	
	$BrO + O \rightarrow Br + O_2$	−2	$BrO_{x-Loss} = 2\times(R_{BrO+O} + R_{BrO+BrO} + R_{BrO+HO2})$
	$BrO + BrO \rightarrow 2\times Br + O_2$	−2	
	$BrO + HO_2 \rightarrow HOBr + O_2$	−2[£]	
	$BrO + ClO \rightarrow Br + Cl + O_2$	−2	$ClO_xBrO_{x-Loss} = 2\times(R_{BrO+ClO}{}^{b} + R_{BrO+ClO}{}^{c})$
	$BrO + ClO \rightarrow BrCl + O_2$	−2	

$O_{x-Loss} = O(3P) + O(1D) + O_3 + NO_2 + 2\times NO_3 + HNO_3 + HO_2NO_2 + 2\times N_2O_5 + ClO + 2\times Cl_2O_2 + 2\times OClO + 2\times CLONO_2 + BrO + 2\times BrONO_2$

[§]R_{A+B} is the reaction rate for reaction A+B→products and J_C is the photodissociation rate constant (i.e. photolysis × concentration) for C+$h\nu$→products. Units are molec.cm^{-3}s^{-1}.

[†]HO_x loss cycles represent a net change $2O_3 \rightarrow 3O_2$ ($\Delta O_x = -2$) due to reactions $OH + O \rightarrow H + O_2$ and $OH + O_3 \rightarrow HO_2 + O_2$. As O_x reactions with OH are faster than with HO_2, only the rate determining steps (RDS) have been considered multiplied by two.

[£]Reactions $XO + HO_2 \rightarrow HOX + O_2$, with X = Cl or Br, have been computed for each family with $\Delta O_x = -2$ because the photolysis of HOX produces an additional O_x loss by the OH radical (i.e. $OH + O_3 \rightarrow HO_2 + O_2$). As these XO + HO_2 reaction are the rate limiting step, their loss rates have been multiplied by two.

Table S4. Halogen heterogeneous reactions on ice-crystals and sulphate aerosols implemented in CAM-chem.

	Reactions	Comments
	Ice-crystal	
Het1	$N_2O_2 + H_2O \rightarrow 2HNO_3$	*
Het2	$ClONO_2 + H_2O \rightarrow HOCl + HNO_3$	*
Het3	$BrONO_2 + H_2O \rightarrow HOBr + HNO_3$	*
Het4	$ClONO_2 + HCl \rightarrow Cl_2 + HNO_3$	*
Het5	$HOCl + HCl \rightarrow Cl_2 + H_2O$	*
Het6	$HOBr + HCl \rightarrow BrCl + H_2O$	*
	Sulfate aerosol reactions	
Het7	$N_2O_2 + H_2O \rightarrow 2HNO_3$	*
Het8	$ClONO_2 + H_2O \rightarrow HOCl + HNO_3$	*
Het9	$BrONO_2 + H_2O \rightarrow HOBr + HNO_3$	*
Het10	$ClONO_2 + HCl \rightarrow Cl_2 + HNO_3$	*
Het11	$HOCl + HCl \rightarrow Cl_2 + H_2O$	*
Het12	$HOBr + HCl \rightarrow BrCl + H_2O$	*

* As in Table A4 from Auxiliary Material in Kinnison et al. (2007). For a complete list of heterogeneous reactions implemented in CAM-chem see Table 4 in the Supplementary Material of Ordoñez et al. (2012).

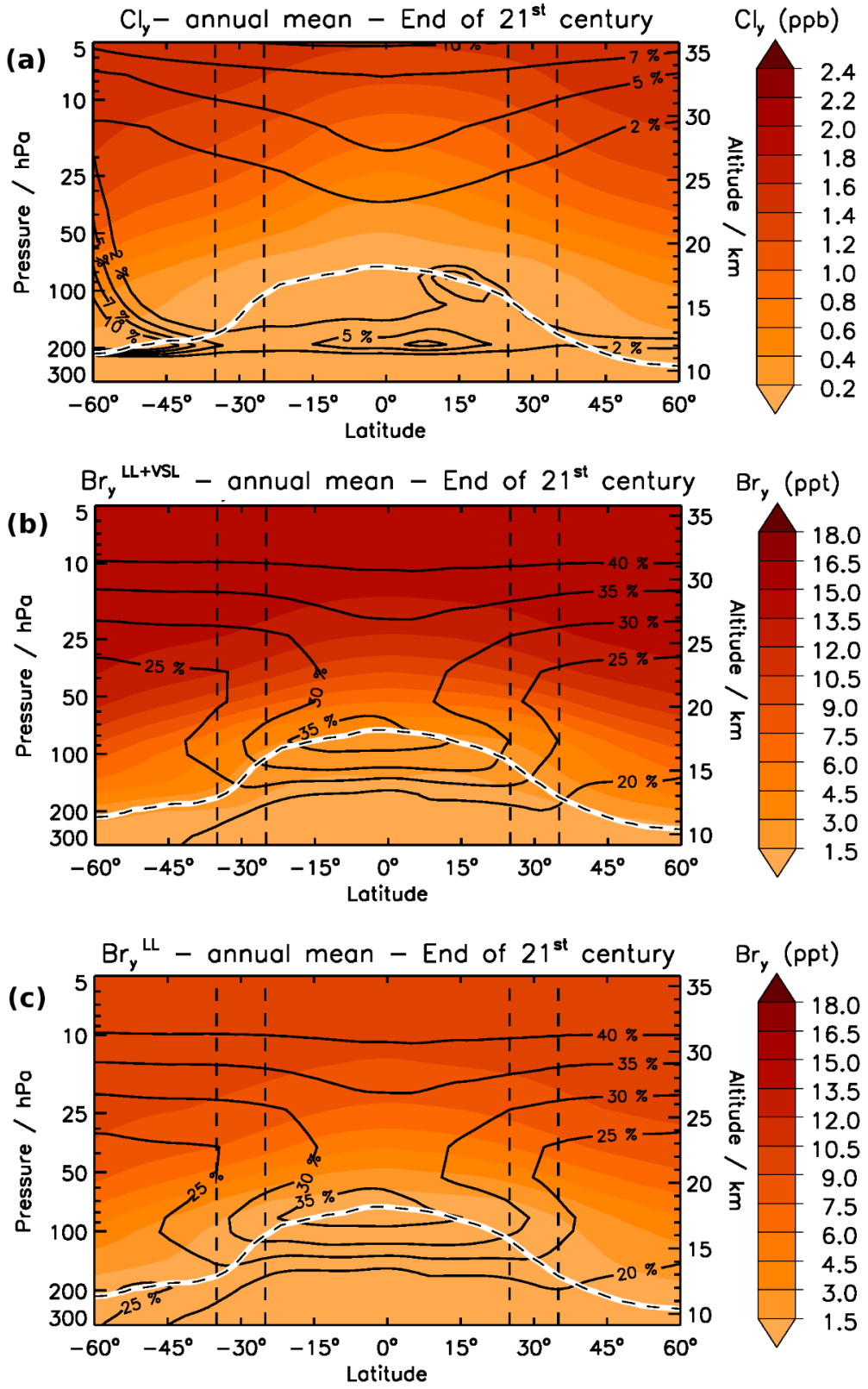

Figure S1: Annual zonal mean distribution of (a) Cl_y^{LL}, (b) Br_y^{LL+VSL} and (c) Br_y^{LL} during the end of the 21st century. The colour scale represents volume mixing ratios (ppb or ppt), while black contour lines show the percentage contribution of ClO_x to Cl_y and BrO_x to Br_y, respectively. The lower solid white line indicates the location of the tropopause (chemical definition of 150 ppb ozone level from experiment without VSL^{Br} sources)

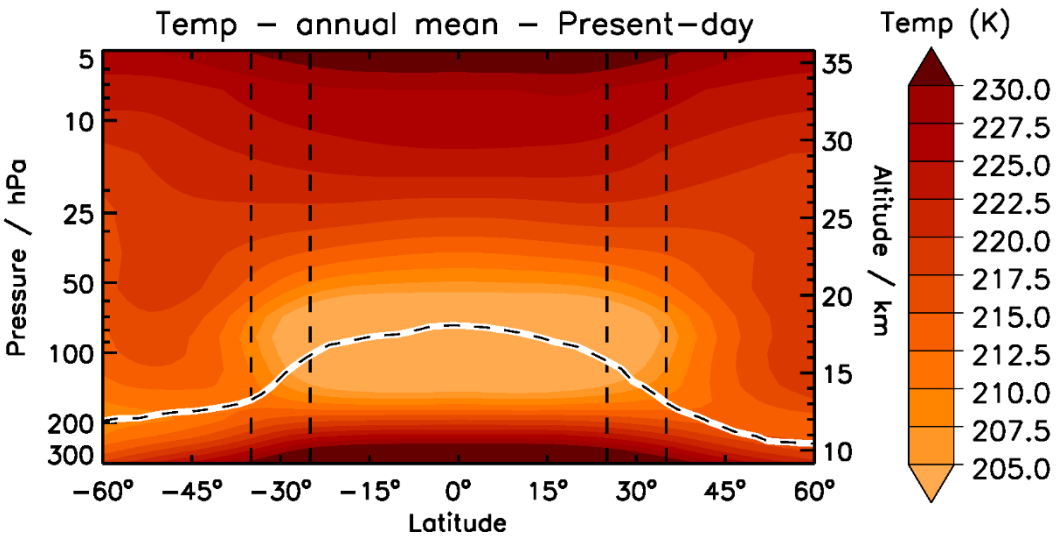

Figure S2: Annual zonal mean Temperature (K) for the present-day period. The lower solid white line indicates the location of the tropopause (chemical definition of 150 ppb ozone level from experiments without VSL^{Br} sources).

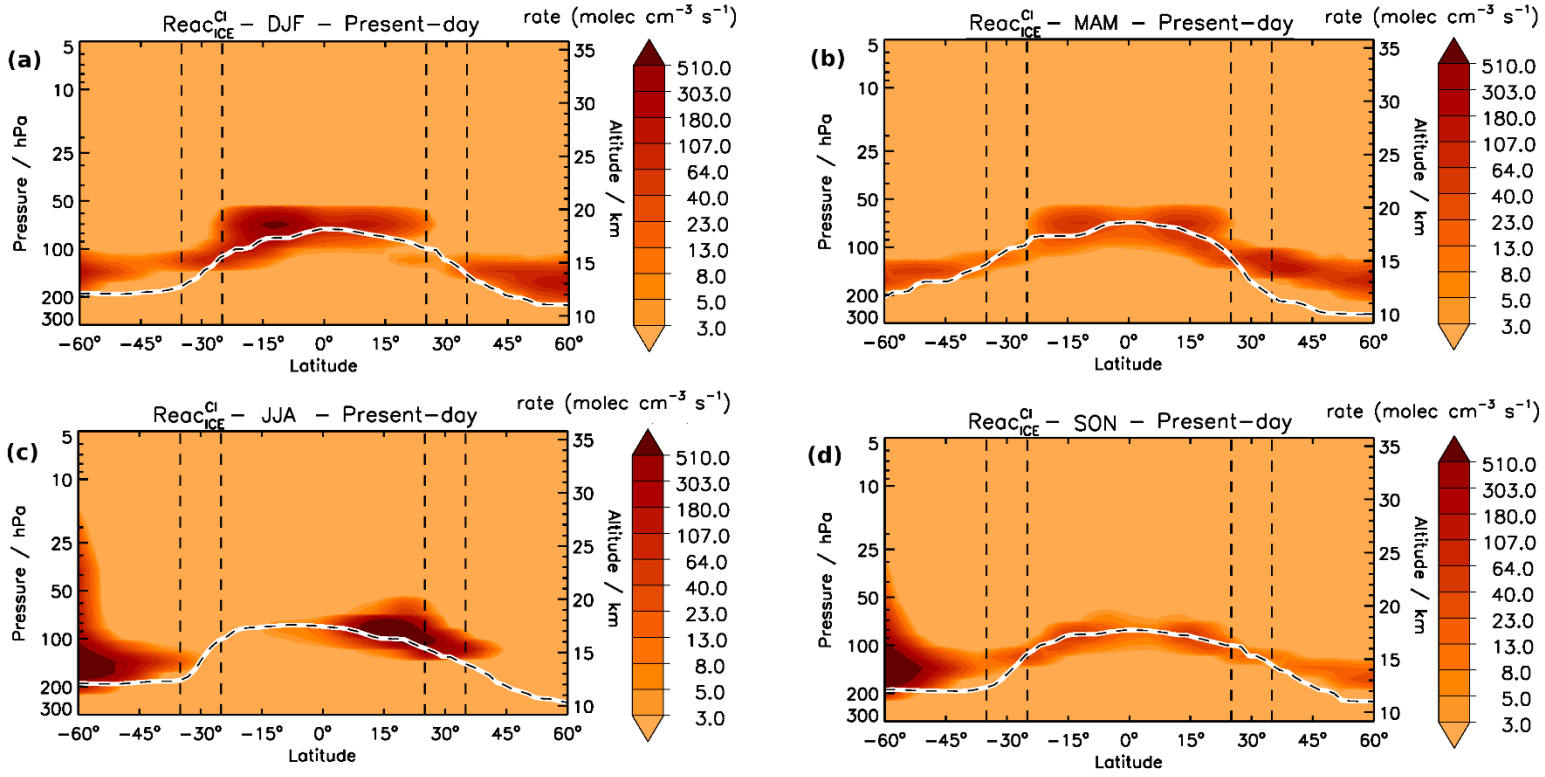

Figure S3: Seasonal zonal mean distribution of the heterogeneous reactivation of chlorine reservoirs ($ClONO_2$ and HCl) on ice-crystal ($Reac^{Cl}_{ICE}$) during the present-day period. The reactions have been specified in Table S4 with the label Het and the corresponding number (i.e. Het 2,4 fo $ClONO_2$ and Het5 for HOCl)

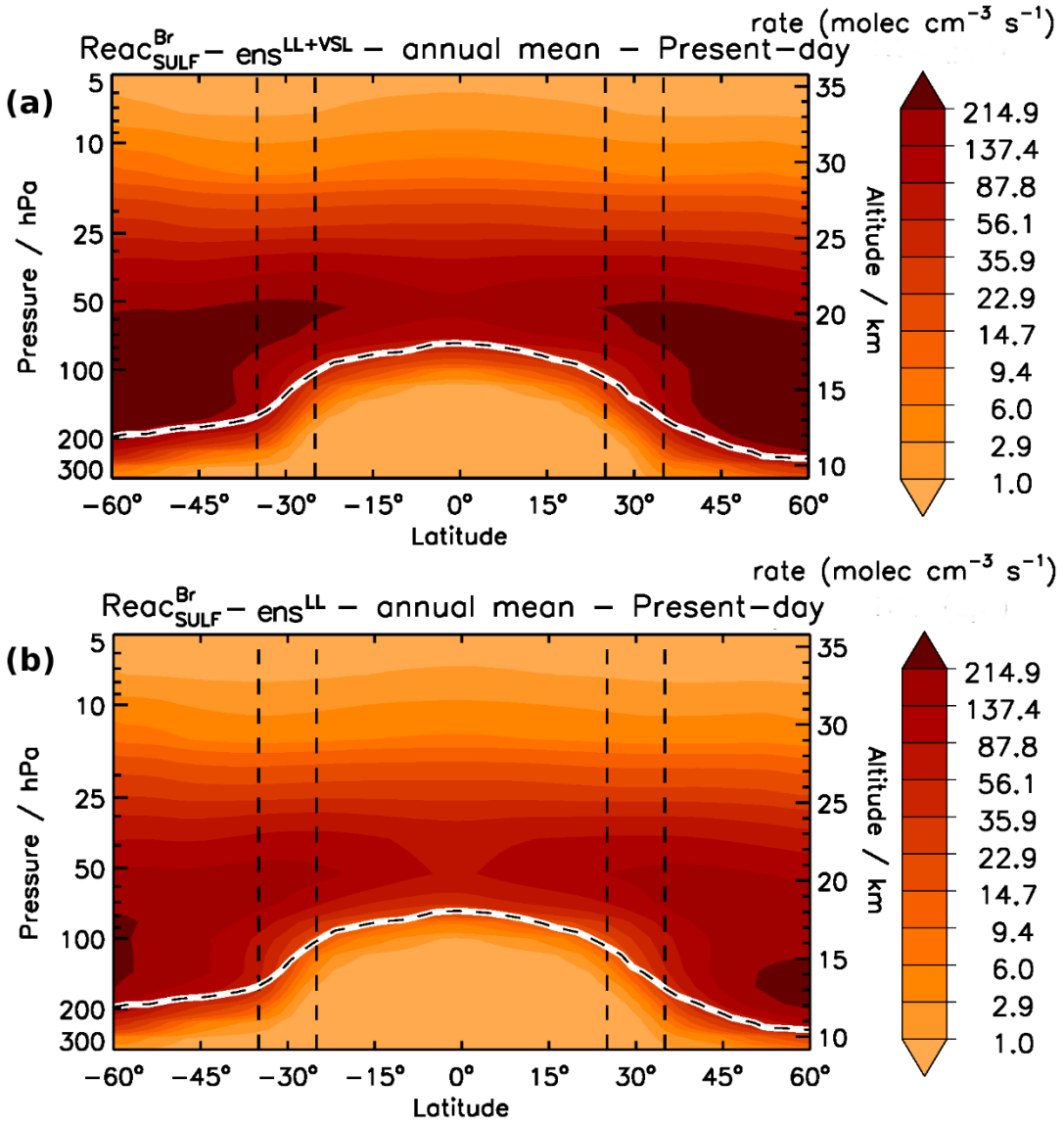

Figure S4: Annual zonal mean distribution of the heterogeneous reactivation of bromine reservoirs ($BrONO_2$ and HOBr) on sulphate aerosols ($Reac^{Br}_{SULF}$) for the experiments (a) with (ens^{LL+VSL}) and (b) without VSL^{Br} sources (ens^{LL}) during the present-day period. The reactions have been specified in Table S4 with the label Het and the corresponding number (i.e. Het9 for $BrONO_2$ and Het12 for HOBr)

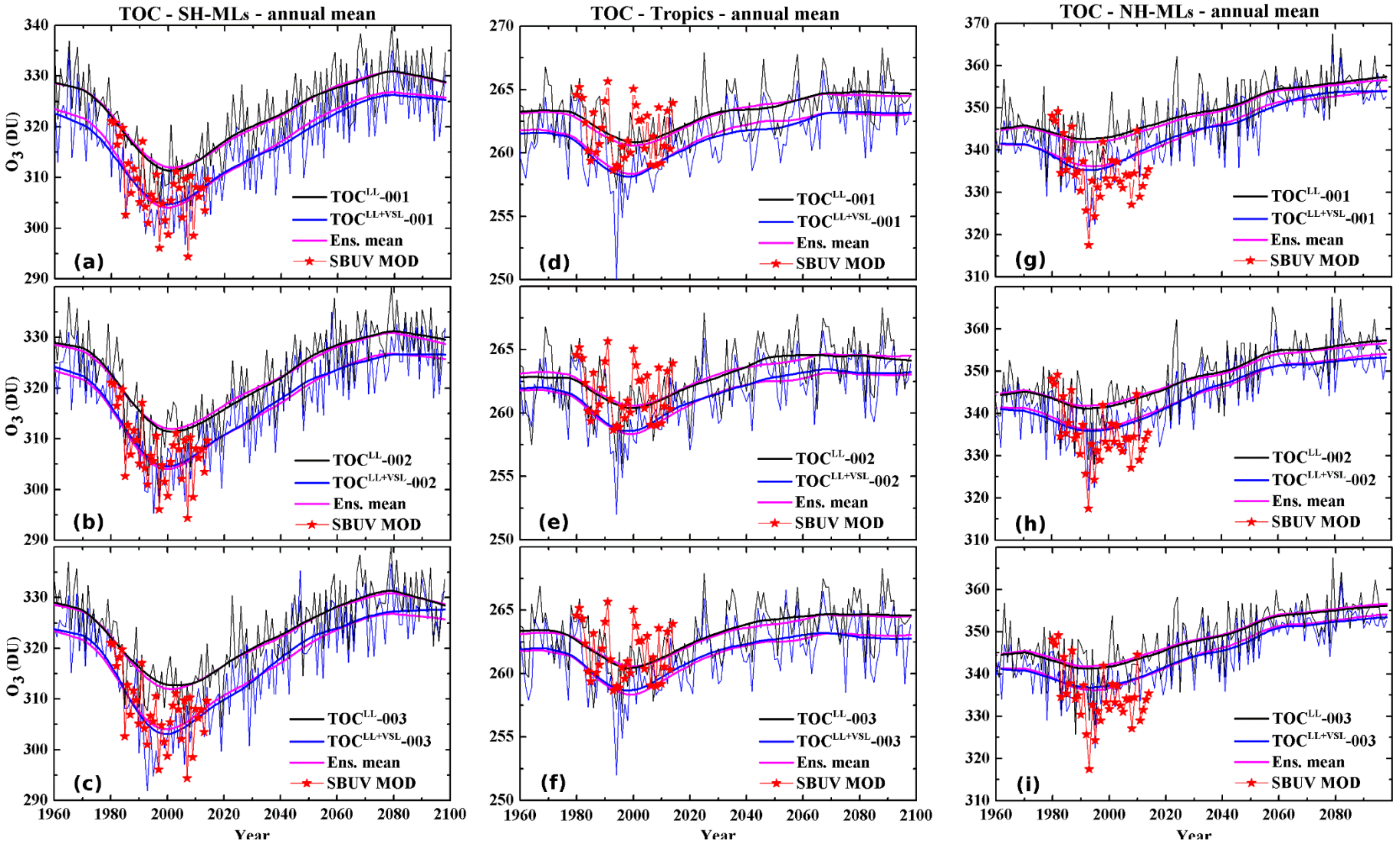

Figure S5: Temporal evolution of the annual mean total ozone column (TOC^{LL+VSL} and TOC^{LL}) for each of the three independent simulations (001, 002, 003; thin lines) of both ensemble experiments within the (a,b,c) SH-MLs, (d,e,f) tropics and (g,h,i) NH-MLs. The time-series smoothed applying a lowess filtering (0.2 fractions; thick lines) are shown in blue for TOC^{LL+VSL}, in black for TOC^{LL} and in pink for the ensemble mean of each experiment. The red lines and symbols show the observations from the Solar Backscatter Ultraviolet (SBUV) merged total ozone column data set (Frith et al., 2014, 2017), within the same spatial and temporal mask as the model output.

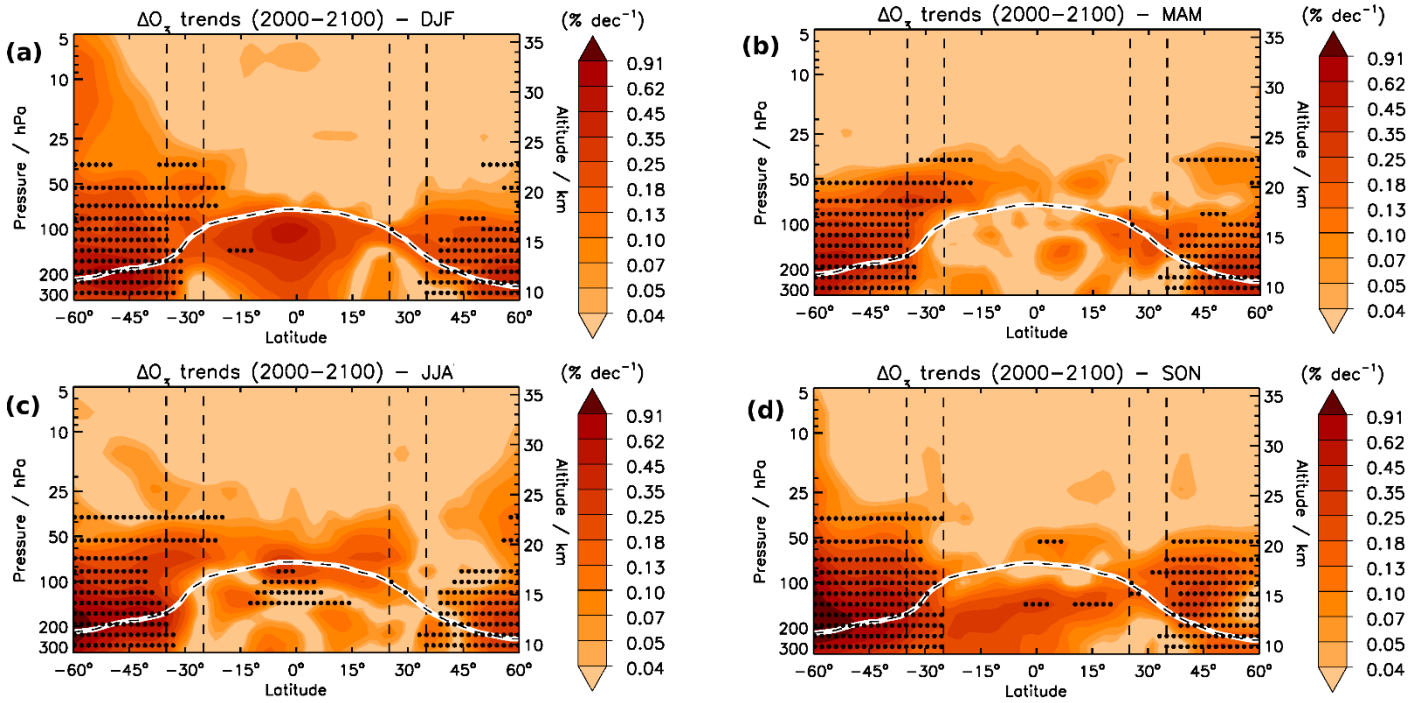

Figure S6: Zonal mean distributions of the seasonal $\Delta O_3(z)$ trends (% dec^{-1}) throughout the century. The masked regions in each panel indicate where the seasonal relative $\Delta O_3(z)$ between the present-day and the end of the 21st century periods are statistically significant at the 95% confidence interval using a two-tailed Student's *t* test.

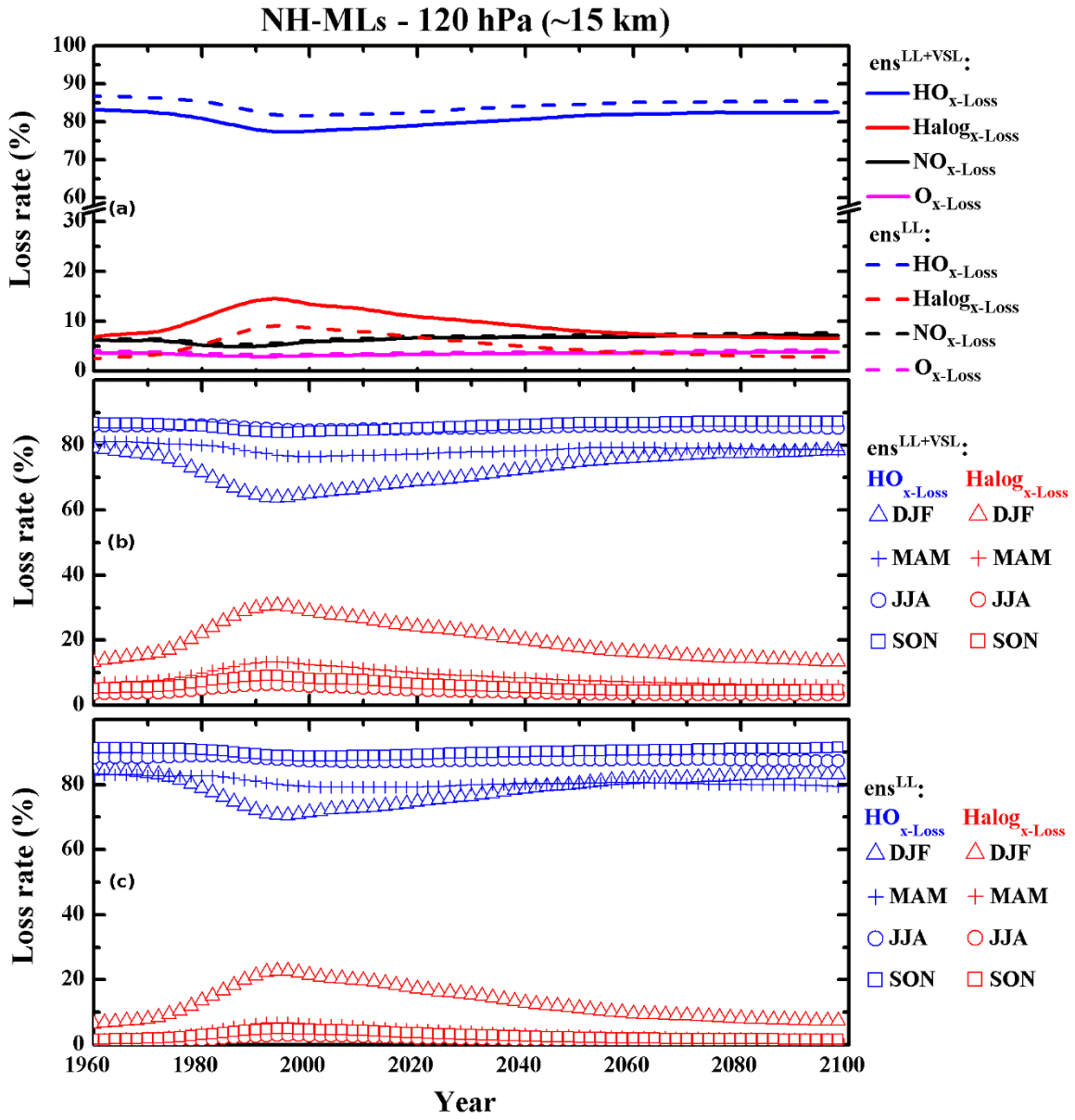

Figure S7: Temporal evolution of the percentage contributions from different ozone-depleting families (O_{x-Loss}, NO_{x-Loss}, HO_{x-Loss}, $Halog_{x-Loss}$) to the total odd-oxygen loss rate in the lowermost stratosphere (120 hPa) at the Northern hemisphere mid-latitudes (NH-MLs). Panel (a) shows the annual mean contribution of each ozone-depleting family for the experiments with (solid line; ens^{LL+VSL}) and without (dashed line; ens^{LL}) VSL^{Br} sources. The panels (b) and (c) show the seasonal mean contributions of both HO_{x-Loss} and $Halog_{x-Loss}$ for the experiments with and without VSL^{Br} sources, respectively.

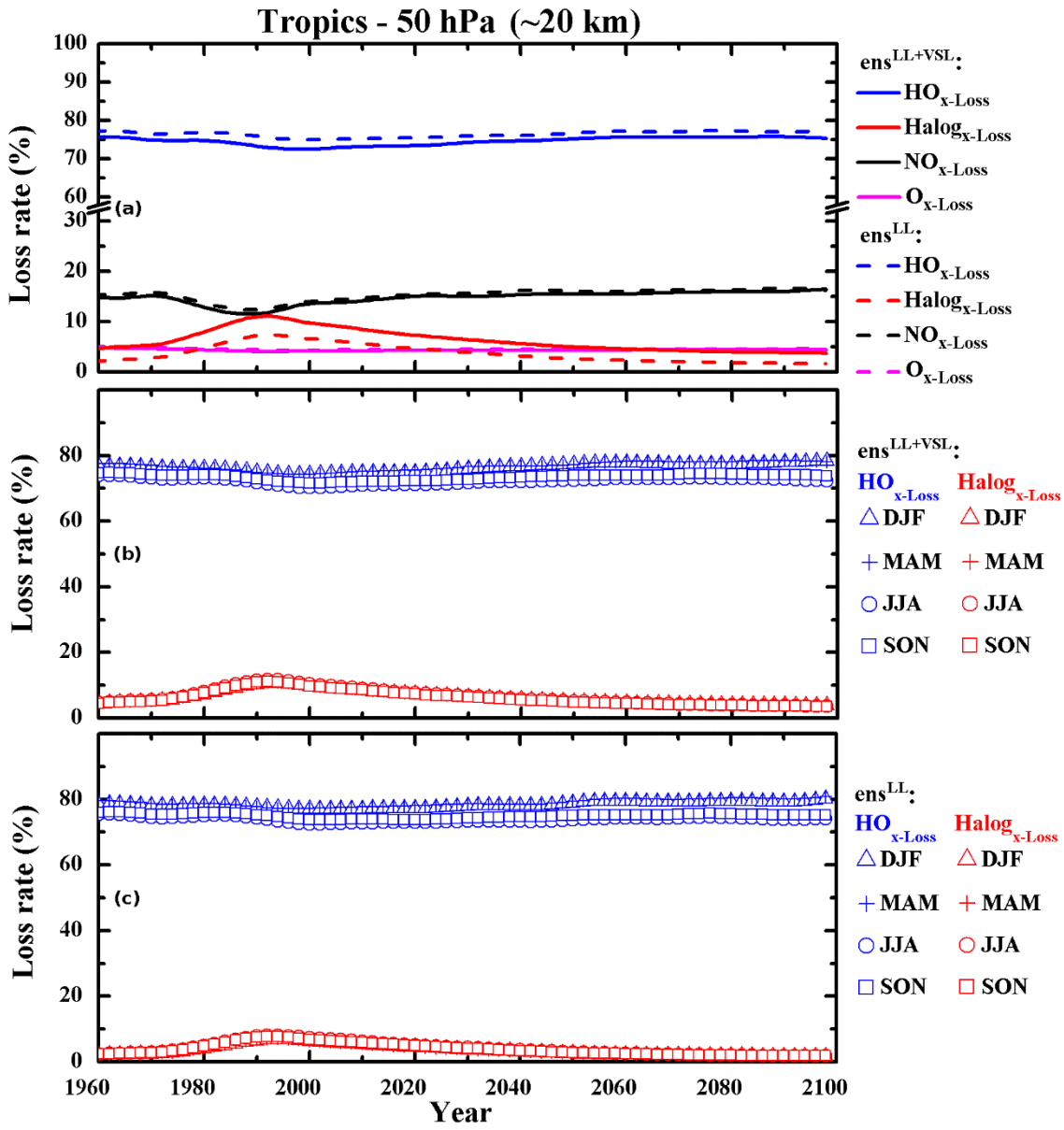

Figure S8: As Fig. S7 but for the lowermost stratosphere (50 hPa) at tropics.

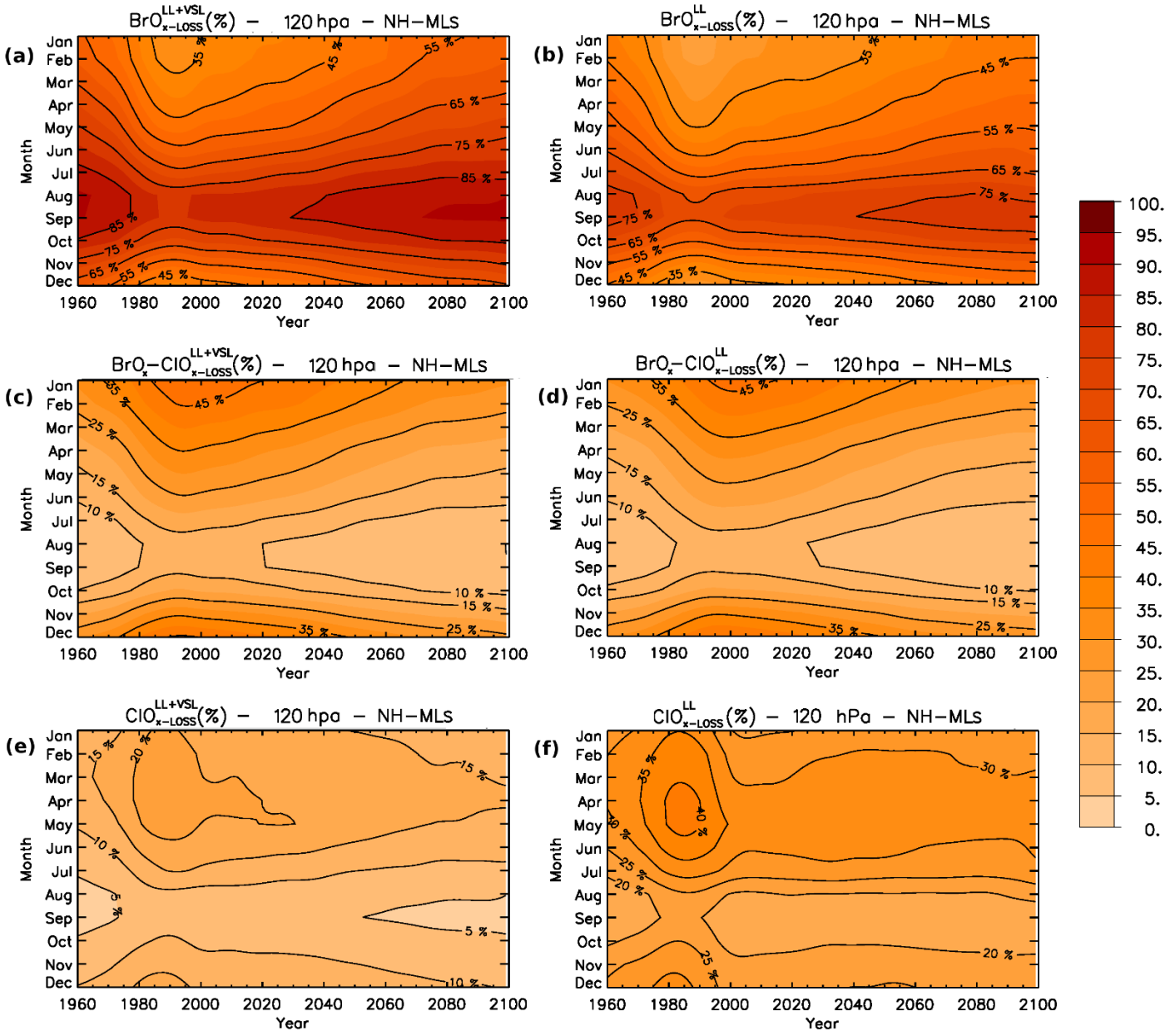

Figure S9: Evolution of the (a,b) BrO_{x-Loss}, (c,d) ClO_x-BrO_{x-Loss} and (e,f) ClO_{x-Loss} percentage contributions to $Halog_{x-Loss}$ as a function of the year and month in the NH-MLs lowermost stratosphere (120 hPa), for the experiments with (left panels) and without (right panel) VSL^{Br} sources.

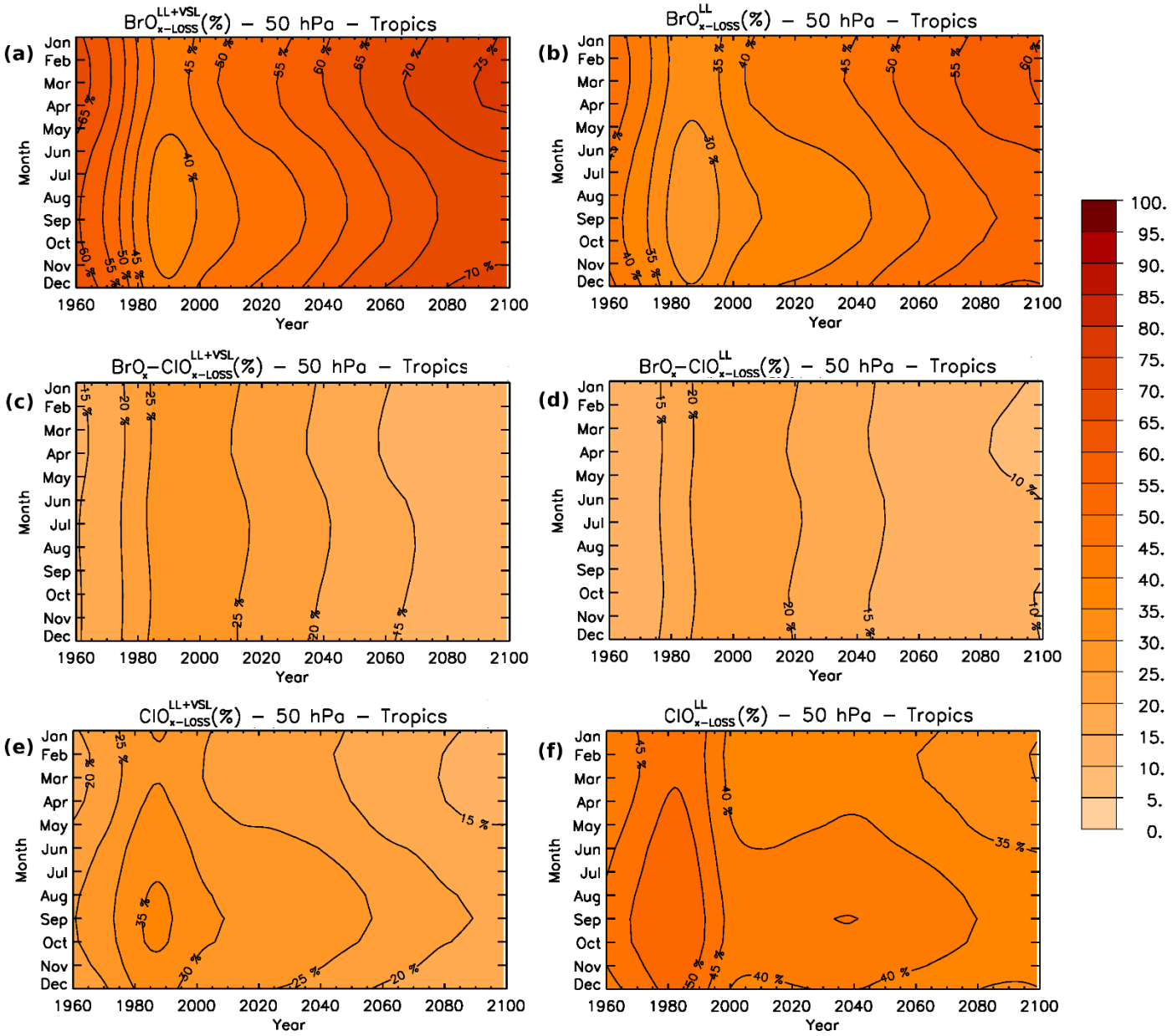

Figure S10: As Fig. S9 but for the lower stratosphere (50 hPa) at tropics.

References

Frith, S. M., Kramarova, N. A., Stolarski, R. S., McPeters, R. D., Bhartia, P. K., and Labow, G. J.: Recent changes in total column ozone based on the SBUV Version 8.6 Merged Ozone Data Set, J. Geophys. Res. Atmos., 119, 9735–9751, https://doi.org/10.1002/2014JD021889, 2014.

Frith, S. M., Stolarski, R. S., Kramarova, N. A., and McPeters, R. D.: Estimating uncertainties in the SBUV Version 8.6 merged profile ozone data set, Atmos. Chem. Phys., 17, 14695–14707, https://doi.org/10.5194/acp–17–14695–2017, 2017.

Kinnison, D. E., Brasseur, G. P., Walters, S., Garcia, R. R., Marsh, D. R., and Sassi, F., Harvey, V. L., Randall, C. E., Emmons, L., Lamarque, J. F., Hess, P., Orlando, J. J., Tie, X. X., Randel, W., Pan, L. L., Gettelman, A., Granier, C., Diehl, T., Niemeier, U., and Simmons, A. J.: Sensitivity of chemical tracers to meteorological parameters in the MOZART-3 chemical transport model, J. Geophys. Res.112, D20302, doi:10.1029/2006JD007879, 2007.

Livesey, N. J., Read, W. G., Wagner, P. A., Froidevaux, L., Lambert, A., Manney, G. L., F., L., Valle, M., Pumphrey, H. C., Santee, M. L., Schwartz, M. J., Wang, S., Fuller, R. A., Jarnot, R. F., Knosp, B. W., Martinez, E., and Lay, R. R.: Version 4.2x Level 2 data quality and description document, JPL D–33509, Rev. D., Jet Propulsion Lab, 2018.

Ordóñez, C., Lamarque, J.-F., Tilmes, S., Kinnison, D. E., Atlas, E. L., Blake, D. R., Sousa Santos, G., Brasseur, G. and Saiz-Lopez, A.: Bromine and iodine chemistry in a global chemistry-climate model: description and evaluation of very short-lived oceanic sources, Atmos. Chem. Phys., 12, 1423–1447, https://doi.org/10.5194/acp–12–1423–2012, 2012.

Waters, J. W., Froidevaux, L., Harwood, R. S., Jarnot, R. F., Pickett, H. M., Read, W. G., Siegel, P. H., Cofield, R. E., Filipiak, M. J., Flower, D. A., Holden, J. R., Lau, G. K., Livesey, N. J., Manney, G. L., Pumphrey, H. C., Santee, M. L., Wu, D. L., Cuddy, D. T., Lay, R. R., Loo, M. S., Perun, V. S., Schwartz, M. J., Stek, P. C., Thurstans, R. P., Boyles, M. A., Chandra, K. M., Chavez, M. C., Chen, G. S., Chudasama, B. V., Dodge, R., Fuller, R. A., Girard, M. A., Jiang, J. H., Jiang, Y., Knosp, B. W., Labelle, R. C., Lam, J. C., Lee, K. A., Miller, D., Oswald, J. E., Patel, N. C., Pukala, D. M., Quintero, O., Scaff, D. M., Van Snyder, W., Tope, M. C., Wagner, P. A., and Walch, M. J.: The Earth Observing System Microwave Limb Sounder (EOS MLS) on the Aura satellite, IEEE T, Geosci. Remote, 44, 1075–1092, https://doi.org/10.1109/TGRS.2006.873771, 2006.